Diamond & Related Materials 69 (2016) 74–80

Contents lists available at ScienceDirect

Diamond & Related Materials

journal homepage: www.elsevier.com/locate/diamond

Molecular dynamics of adhesion force of single-walled carbon nanotubes

Jian Liu [a], Xiaobin Tang [a,b,*], Feida Chen [a], Hai Huang [a], Huan Li [a], Da Chen [a,b]

[a] Department of Nuclear Science & Engineering, Nanjing University of Aeronautics and Astronautics, Nanjing 210016, China
[b] Jiangsu Key Laboratory of Nuclear Energy Equipment Materials Engineering, Nanjing 210016, China

ARTICLE INFO

Article history:
Received 24 December 2015
Received in revised form 14 June 2016
Accepted 18 July 2016
Available online 20 July 2016

Keywords:
Carbon nanotube
Adhesion force
Irradiation induced defects
Molecular dynamics

ABSTRACT

It is of great significance to provide theoretical guidance to the application of carbon nanotubes as adhesive materials via the investigation on their adhesion force. In this paper, molecular dynamics was adopted to investigate the adhesion force between the graphene substrate and the carbon nanotubes with varying deformation degrees and diverse types of irradiation induced defects at different temperatures. No obvious adhesion force was found between the carbon nanotube and graphene until the deformation degree of the former reached >70%. The adhesion force would be maintained at a high level when the temperature was in the range of 280–320 K, which limited its application. Moreover, the adhesion force between carbon nanotube with vacancies and graphene substrate would decrease with increasing size of vacancies. Finally, compared with monovacancies and divacancies, Stone-Wales defects most remarkably reduced the adhesion force of carbon nanotubes.

1. Introduction

In nature, gecko lizards can adhere to nearly any object [1]. Bionics has shown that this ability of gecko lizards is related to the setae on their feet [2,3]. Inspired by this phenomenon, scientists have discovered that a carbon nanotube (CNT) array has the same adhesive capacity, thereby making it a promising adhesive material for future space robots [4–7]. Fig. 1 from Ref. [8] demonstrates the microscopic pictures of a gecko foot and a CNT array.

Among the reported literature, theoretical derivation and experiments are mainly adopted to research the adhesion force of CNT. Leckband et al. [9] theoretically deduced the van der Waals force of cylinder near a flat surface. Buchoux et al. [10] and Li et al. [11] took the advantage of atomic force microscope (AFM) to investigate the mechanical behavior and adhesion energy per unit length of a single-walled CNT on various substrates. Zhao et al. [12] and Qu et al. [13] investigated the adhesive strengths in the normal direction and shear direction with glass surface both theoretically and experimentally. In recent years, some researchers have shown their interest in simulation. For example, Buldum [14] studied adhesion behavior and characteristics of CNT by computer simulation by molecular dynamics (MD).

Investigations done by predecessors have already contributed to a deeper understanding of the characteristics of the adhesion force of perfect CNT. However, the introduction of defects on a perfect CNT wall is inevitable in practice during the fabrication and application of CNT arrays. In particular, high energy rays and particles will surely hit surface atoms when applied in space in the future [15,16], which could change the surface structure of the CNTs and form defects [17,18]. The existence of defects may cause significant variation in the adhesion force of CNT. Therefore, an appropriate approach must be found to study the change in the adhesion force of the CNT under such circumstances. MD can be used to simulate the evolution of the CNT structure before and after irradiation on atomic scale. Successful examples of MD simulations have been reported to explore deformation and failure of CNT [19,20]. Consequently, MD was adopted to simulate the adhesive behavior and to calculate the adhesion force of CNTs with different deformation degrees, temperatures, vacancy sizes, and defect types. The effects of these conditions on the adhesion force of CNTs were also discussed.

2. Model and method

2.1. CNT adhesion process

In the previous CNT adhesion experiments described above, the total adhesion process can be broken down into three basic steps. First, the CNT is forced to move toward to the object until the front part of CNT contacts its surface. At the end of this step, the van der Waals force between the CNT and the surface is 0. Second, a pre-stress is exerted on the CNT to deform its front portion. At this moment, the front portion of CNT is assumed to deform and flatten by the pre-stress from a microscopic view. Third, the pre-stress is removed while the contact portion of the CNT still remains deformed and will not return to its original shape. Under such conditions, the deformed part will firmly adhere to the object and generate a strong adhesion force along the shear direction, as

* Corresponding author at: Department of Nuclear Science & Engineering, Nanjing University of Aeronautics and Astronautics, Nanjing 210016, China.
E-mail address: tangxiaobin@nuaa.edu.cn (X. Tang).

http://dx.doi.org/10.1016/j.diamond.2016.07.009
0925-9635/

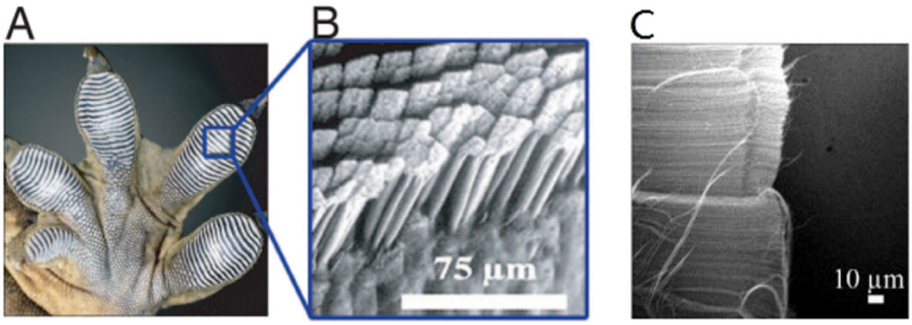

Fig. 1. (A) Optical picture of gecko foot showing that the setae are arranged in many lobes along the foot. (B) SEM image of natural gecko setae terminating into thousands of smaller spatulas. (C) A SEM picture of the edge of tape where the deformation of the carbon nanotubes after it has been pressed in contact with the mica surface was observed. The edge observed in the middle of the SEM picture is the boundary between the carbon nanotubes and the substrate.
Reprinted with permission from Ref. [8]. Copyright (2007) National Academy of Sciences.

shown in Fig. 2(a). Based on the above analysis, it is easy to find out that the adhesion force of CNT comes from the van der Waals force between atoms of contact portion of the CNT and atoms on the surface of the object, due to the appropriate distance between them. This theory has been experimentally proved by some researchers [10–13]. Consequently, the deformed part of CNT is called the effective contact area, where the adhesion force is exclusively generated, as shown in Fig. 2(b). Therefore, the emphasis of this paper is the effective contact area and not the entire CNT.

According to the practical microscopic contact behavior described above, a simulation of pre-stress exerted on the CNT was carried out and subsequently the adhesion force between the deformed CNT and the substrate was measured.

2.2. Simulation model and method

Before the simulation, a sandwich structure model was established, as shown in Fig. 3. A single layer of graphene was placed on the top and bottom parts of the model. Both layers of graphene were exactly the same in the x and y coordinates and only differed in their z coordinates. In the middle of the sandwich model, a 100 nm long armchair single-walled CNT (SWCNT) with chirality of (10, 10) lay along the y-axis. The graphene was large enough to completely cover the CNT. Graphene was constructed and placed in such a position to control the precise deformation of the CNT. Lower levels of graphene could serve as substrate, which would be adhered to the CNT.

After modeling, the upper graphene layer was moved downward manually with the velocity of 4.92 nm/ps to compress the CNT. Though the adhesion force investigated in Ref. [6] (Fig. 2(a)) seems to be generated by the buckling-induced loading, the essence and results of two different ways treating the CNT, buckling-induced loading and directly compressing, are the same since the adhesion force is generated actually due to the van der Waals interaction between substrate atoms and CNT atoms, which only shows up when the distance of two atoms is close enough. Since the purpose of the CNT deforming and the buckling-induced loading is only to make the distance as close as possible to generate effective adhesion force, their final effects are equivalent.

At the end of compressing, the CNT had deformed to some degree, as shown in Fig. 4, and after that, the upper graphene atoms were deleted. On account of the difficulty of precise calculating the effective contact area, the deformation degree was used instead. The deformation degree in this paper was defined as the following formula:

$$\delta = (1-h/D) \times 100\% \tag{1}$$

where h is the maximum height of the deformed CNT along the z-axis, and D is the diameter of original CNT.

Notably, the CNT would not return to its original state and remained the deformed shape. To produce adhesion force between the CNT and graphene substrate, the deformed CNT was dragged along its axial direction after 20 ps relaxation. The dragging force was 0.16 nN per CNT atom and therefore, a total dragging force of 2.61 μN was exerted on the whole deformed CNT. Since the upper graphene atoms were deleted, the pre-stress was accordingly removed. In addition, the effects of the pre-stress on the deformed CNT had been eliminated completely after the 20 ps relaxation. According to the famous friction formula:

$$F = \mu \times F_N \tag{2}$$

where F is the friction force, μ is coefficient of kinetic friction and F_N is normal compressive force, since neither pre-stress (i.e., compressive

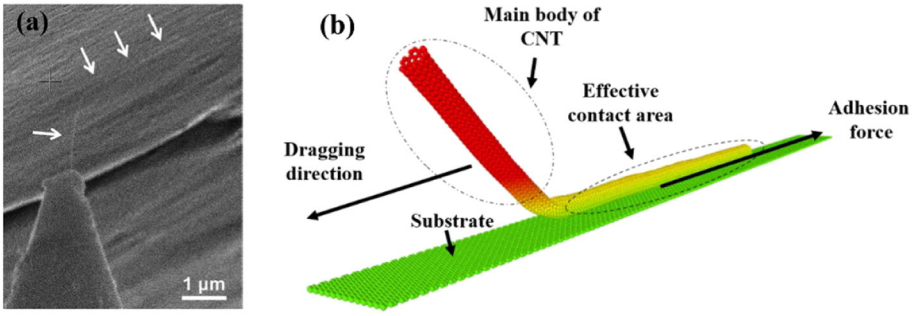

Fig. 2. (a) SEM image of a CNT welded to a cantilever tip and in contact with a graphene surface. Arrows denote the path of the CNT, including the line contact beneath the three top arrows. *Reprinted with permission from Ref. [6]. Copyright (2014) American Chemical Society.* (b) Schematic of CNT contacting substrate. Carbon atoms are colored according to their regions. (For interpretation of the references to color in this figure legend, the reader is referred to the web version of this article.)

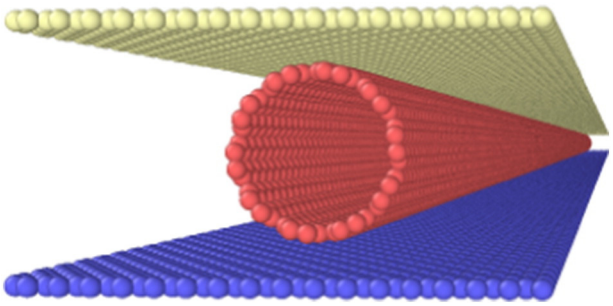

Fig. 3. Sandwich-like geometric model of CNT covered with two graphene layers. Yellow and blue carbon atoms in this figure represent graphene at the top and bottom of the model, respectively. Red carbon atoms constitute the CNT. (For interpretation of the references to color in this figure legend, the reader is referred to the web version of this article.)

force) nor effects of it acted on the deformed CNT after relaxation, the force generated by the dragged CNT and the substrate graphene was adhesion force rather than friction force. For all the simulations in this paper, the temperature was set to 300 K, except for investigating the temperature influence on the adhesion force, when the temperature ranged from 100 to 400 K.

The classical MD simulation software LAMMPS was employed in this paper. This software was developed by Sandia National Laboratories in USA [21]. The selection of the potential function considerably affected the MD simulation results. Only carbon atoms were present in this simulation system and the CNTs of carbon atoms were in a condensed state as well as graphene. Thus, the Adaptive Intermolecular Reactive Empirical Bond Order (AIREBO) potential [22], which is widely used to describe the precise interaction of a hydrocarbon system, was adopted in this paper, which is expressed as follows:

$$E = \frac{1}{2}\sum_{i}\sum_{j\neq 1}\left(E_{ij}^{\mathrm{REBO}} + E_{ij}^{\mathrm{LJ}}\right) \tag{3}$$

where i and j are the serial numbers of the atoms. The first term in the parenthesis is the Reactive Empirical Bond Order (REBO) potential developed by Brenner [23–25], which can only describe short-ranged carbon–carbon (C—C) interaction and is expressed as follows:

$$E_{ij}^{\mathrm{REBO}} = V_{ij}^{\mathrm{R}}(r_{ij}) + b_{ij}V_{ij}^{\mathrm{A}}(r_{ij}) \tag{4}$$

where b_{ij} is the multiple–body bond order term, V_{ij}^{R} and V_{ij}^{A} are the repulsive and attractive pairwise potentials, respectively, which depend on the distance r_{ij} between the two atoms. The second term in the parenthesis of Eq. (3) can be used to describe the long-ranged C—C interaction known as a van der Waals interaction. Given its similar form to the Lennard–Jones (LJ) potential function, Eq. (3) can be approximately expressed as follows [22]:

$$E_{ij}^{\mathrm{LJ}} = 4\varepsilon_{ij}\left[(\sigma_{ij}/r_{ij})^{12} - (\sigma_{ij}/r_{ij})^{6}\right] \tag{5}$$

where ε_{ij} and σ_{ij} are only related to the atomic type, and are constant in this simulation. Consequently, the van der Waals interaction in this paper only involved the distance between atoms. The velocity Verlet algorithm was applied to integrate the equations of motion [26], and the adhesion force was obtained as time averages over the particle positions and velocities [27].

3. Results and discussion

3.1. Deformation degree

In this section, the adhesion force between CNTs of various deformation degrees and the graphene substrate was studied. Fig. 5 shows the adhesion force as a function of the CNT deformation degree, which shows that the adhesion force is nearly negligible and will not show up until the deformation degree reaches >70%. When the CNT deforms slightly, the distance between the C atoms on the bottom of the CNT and graphene substrate is too large to generate an effective van der Waals force, thus, the adhesion force is weak. As the deformation goes on, the degree increases and finally, the critical degree is exceeded. In this circumstance, the distance between the bottom of the CNT and the graphene substrate is less than the critical value. At this time, the van der Waals force is large enough to macroscopically appear as the adhesion force.

After the CNT deformation degree exceeds 70%, the adhesion force of CNT seems to ascend dramatically. To investigate the relationship between the adhesion force and the deformation degree, the deformation degree within the range 75% to 82.5% is determined. As shown in Fig. 6, the adhesion force of the CNT nonlinearly increases with increasing deformation degree, and the trend fits the cubic curve plotted in the diagram. The specific expression of the cubic curve is as follows:

$$F = -50669 + k_1 \times x + k_2 \times x^2 + k_3 \times x^3 \tag{6}$$

where x is the deformation degree, k_1, k_2, and k_3 are 195,249, −250,847, and 107,466 nN, respectively. When the distance between the CNT and the graphene substrate is slightly less than the critical value, the C atoms on the bottom of the CNT are subject to a repulsive force generated by the graphene layer, which may increase in the distance between the CNT and substrate. Therefore, the increasing adhesion force is smooth at the initial stage of adhesion force growth, thereby corresponding to the negative value of the quadratic term coefficient k_2 in Eq. (6).

Figs. 5 and 6 show the adhesion force of a single CNT. A CNT array consists of aligned CNTs, which are usually fabricated and used in practical applications. Thus, the adhesion force of a CNT array can be theoretically calculated as follows:

$$P = F \times \rho \tag{7}$$

where F is the adhesion force of the single CNT, ρ is number density of CNT array, which is ~10^{10} cm^{-2}. When the CNT deformation degree is 80%, F is 11.35 nN. According to Eq. (7), the adhesion force of the CNT array is 113.5 N/cm^2, which is comparable to the value of 97 N/cm^2 obtained from the experiment conducted by Qu et al. [13]. For convenience, the deformation degree was kept at 80% to investigate other effects on the CNT adhesion force.

3.2. Temperature

As shown in Fig. 7, the adhesion force of CNT in different temperatures was studied. The temperature shown in the figure ranges from 100 K to 400 K and increases every 20 K. Fig. 7 clearly shows that with

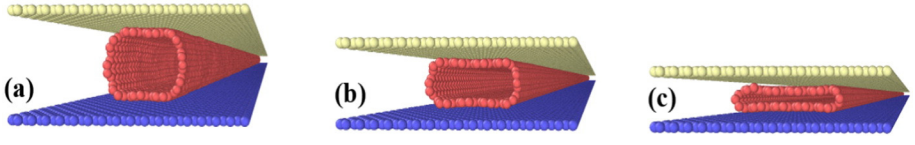

Fig. 4. Schematic model of graphene and CNT with different deformation degrees: (a) 20%, (b) 50%, and (c) 80%, respectively.

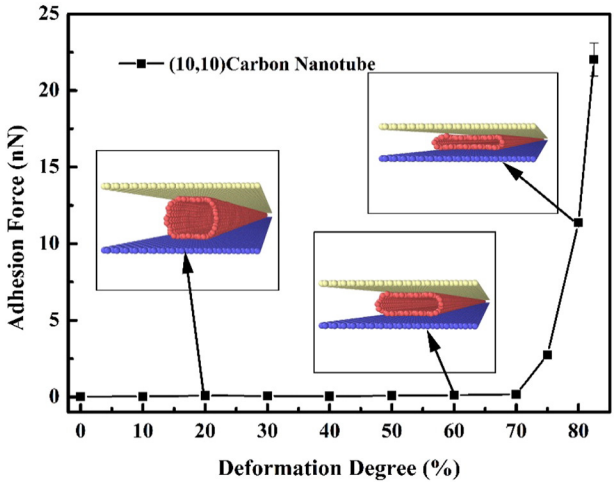

Fig. 5. Adhesion force of CNTs as a function of the deformation degree. Insets are schematic models of graphene and CNTs according to the deformation degree.

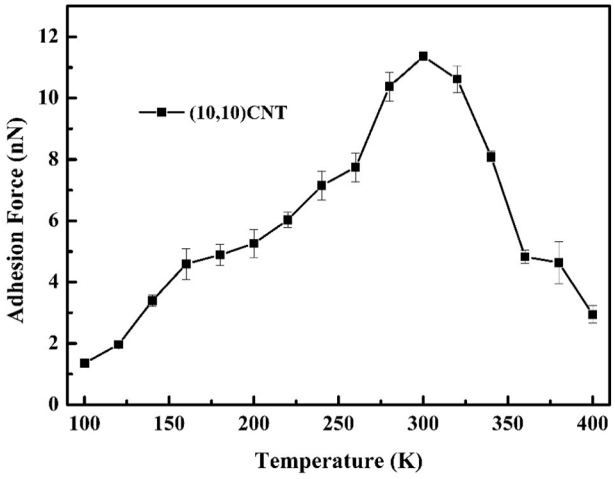

Fig. 7. Adhesion force of CNTs as a function of temperature.

the same deformation degree, the adhesion force of CNT increases with increasing temperature and reaches its maximum value at 300 K. Nevertheless, the adhesion force rapidly drops while the temperature continues to increase beyond 300 K. This phenomenon occurs because of the atomic energy. Microscopically, the level of atomic vibration represents the temperature of the macroscopic objects that contain it. The more strongly the atoms vibrate, the higher the temperature is. Although the deformation degree was kept 80% as mentioned above, the average degree for the whole CNT was studied in this paper. As the temperature increases from 100 K, which corresponds to more strenuous atomic vibration, more and more atoms come close to the substrate, thereby increasing the adhesion force. Having got too much energy for vibration at high temperature >300 K, however, atoms on the bottom of the CNT tend to migrate to the equilibrium position, where the distance between atoms and the substrate is farther than that at 300 K, to keep their energy at the minimum. The distance becomes larger and even exceeds beyond the critical value, which causes the sharp decrease of adhesion force at high temperature. As seen from Fig. 7, the adhesion force of CNTs can be kept at a high level within the range 280–320 K, which limits the applications of a CNT array.

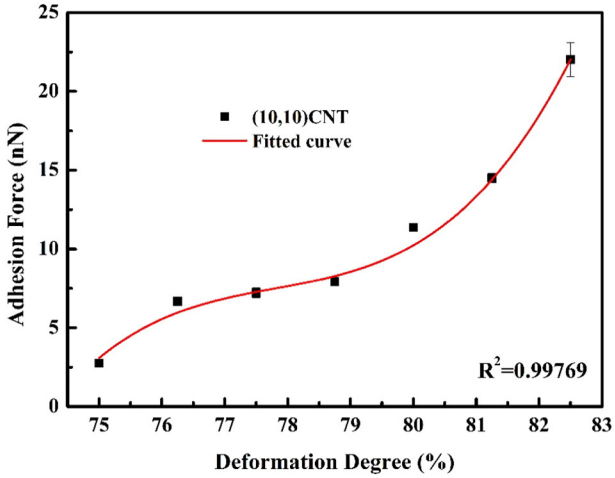

Fig. 6. Closer look at the adhesion force as a function of CNT deformation degree.

3.3. Vacancy size

During the practical application of CNT arrays, defects are bound to be generated. Furthermore, when possibly applied in space in the future, CNTs will be exposed to high-energy rays and swift particle irradiation, which would interact with the atoms of CNTs, thereby producing numerous defects on the CNT wall. In addition, a perfect CNT (i.e., without defects) cannot be fabricated in practice. The alteration of the topology and structure of CNTs caused by the defects may result in the variation of the adhesion force. Therefore, the relationship between adhesion force of CNT and defects should be studied. In this subsection and the next, the effects of defects on the adhesion force are discussed. For convenience, all defects are assumed to be located in the bottom of CNT.

Fig. 8 shows several different diagrammatic cross-sections of CNTs containing defects. All the defects are assumed to gather together to form a large vacancy at the bottom of the CNT. The number of lost atoms instead of the diameter of the vacancy can be used to describe the vacancy size. Obviously, larger vacancy size corresponds to more lost atoms. From Fig. 9, which shows the adhesion force as a function of the number of lost atoms, it is easy to discover that the adhesion force decreases approximately linearly with the increase of the number of lost atoms (i.e., the vacancy size). The main reason for the phenomenon described above is the effective contact area, which is bound to shrink with expanding vacancy size, thereby resulting in the reduction of the van der Waals force. After long-term service, vacancy size on the CNT wall will be surely enlarged. Consequently, to keep the adhesion force, vacancy size is not a negligible factor to consider.

3.4. Defect type

As discussed in references [28,29], most of the well-known and well-studied defects are monovacancies, divacancies and Stone-Wales (S-W) defects. Monovacancy is the vacancy type with a structure that results from the removal of a single C atom on the CNT wall, as shown in Fig. 10(a). Similarly, a divacancy refers the structure where two neighboring atoms are removed from the CNT wall, as shown in Fig. 10(b). The S-W defect does not result from atom loss but from the topological transformation of C atoms on the CNT wall during and after irradiation, as shown in Fig. 10(c). The rotation of a C—C chemical bond by 90° [30] will lead to the formation of two heptagons and two pentagons, which replaces the original four hexagons surrounding them, and this type of defect with such a topological structure is called an S-W defect.

Fig. 11 shows the adhesion force of CNTs containing different defect types as a function of the defect concentration. When investigating a

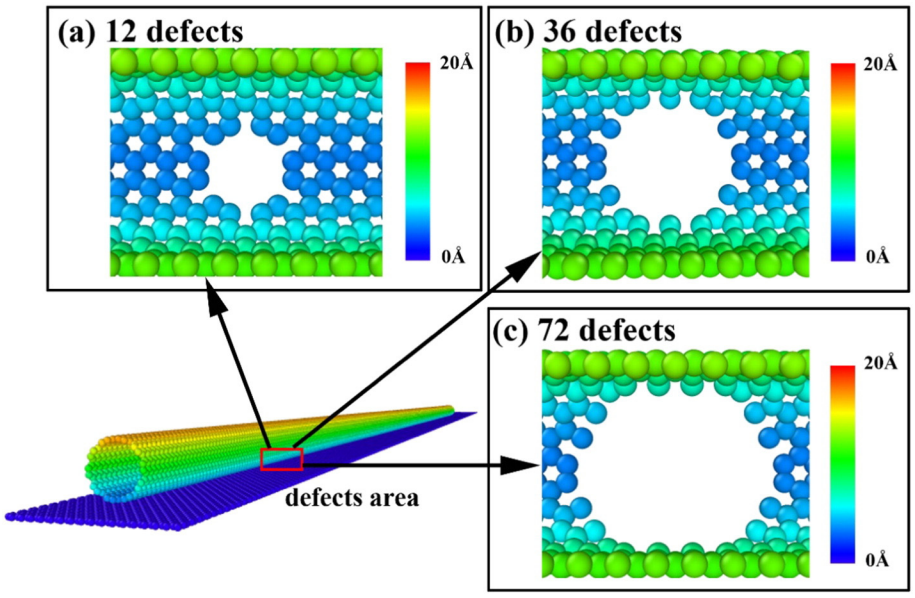

Fig. 8. Diagrammatic cross-section of CNTs with different defects. (a), (b) and (c) correspond to 12, 36 and 72 defects, respectively. Carbon atoms are colored according to their *z*-coordinates. (For interpretation of the references to color in this figure legend, the reader is referred to the web version of this article.)

certain kind of defect type, the CNT model only contained this type. Regardless of the defect type in the CNT, Fig. 11 shows that the adhesion force decreases as the defect concentration increases. When the defect concentration is constant, the CNTs with monovacancies have the maximum adhesion force, followed by the CNT with divacancies. Finally, the CNT with S-W defects has the lowest adhesion force. Furthermore, the latter greatly differs from the corresponding adhesion force of other two kinds of defects.

The formation of monovacancies or divacancies resulting from the absence of C atoms on the CNT wall leaves C atoms of coordination numbers <3, which surround the vacancies. During the compression of CNTs, these atoms with unsaturated dangling bonds partially combine with each other and form new C—C covalent bonds. The other part of these atoms interacts with the C atoms on the substrate by forming chemical bonds, which compensates for the loss of adhesion force caused by the lack of the original C atoms. Additionally, when a single monovacancy appears, the ratio of the number of dangling bonds to lost atoms is 3 to 1 but this ratio becomes 4 to 2 when a single divacancy shows up. Therefore, monovacancies compensate more than divacancies, thereby causing the adhesion force of CNTs with monovacancies to be greater than that of those with divacancies.

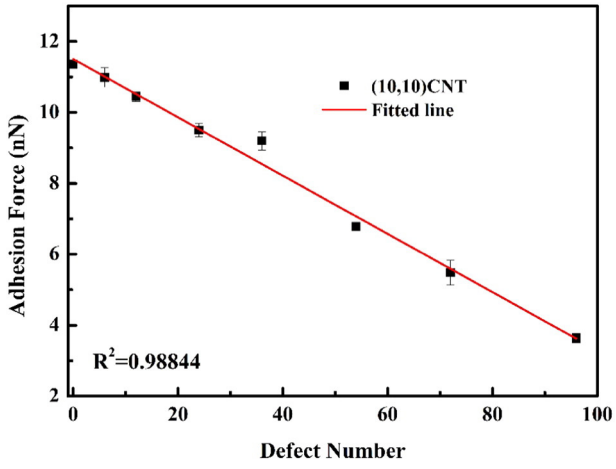

Fig. 9. Adhesion force of CNTs as a function of the number of lost atoms.

Given the shrinkage of the effective contact area, the S-W defects reduce the adhesion force of CNTs. Nonetheless, the S-W defect is a perfect structural defect, that is, all the C atoms are perfectly matched and have no dangling bonds. The compensation effect on the adhesion force is minimal, thus, the adhesion force of the CNT with S-W defects is much lower than that of the other two types of defects.

4. Conclusions

In this study, MD was conducted to investigate the adhesion force between armchair single-walled CNT and graphene substrate under different conditions. The influence of various factors on the adhesion force was also discussed and the following conclusions were obtained.

(1) The effective adhesion force will not appear until the deformation degree of perfect CNT exceeds 70%. In such a condition, the adhesion force well matches the deformation degree in the form of the cubic curve.
(2) The adhesion force of perfect CNT will first increase and then decrease with the increase of temperature from 100 K to 400 K, and its maximum value is reached at 300 K. In the range of 280–320 K, the adhesion force will remain high.
(3) The adhesion force of CNT containing vacancies almost linearly decreases as the vacancy size expands. With time, the vacancy size of the CNT will surely increase because of irradiation of high energy rays and swift particles. Therefore, the exposure time of CNTs should be considered before irradiation is applied.
(4) When monovacancies, divacancies or S-W defects exist in the CNT, its adhesion force will decrease with the increased defect concentration for all three conditions. The dangling bonds have compensatory effect. The CNT with monovacancies has the highest adhesion force, followed by the CNT with divacancies and the CNT with S-W defects when the defect concentration is constant.

Based on the abovementioned conclusions, a theoretical guide can be provided for utilizing CNTs as adhesive materials. Further studies on more complicated situations, such as the CNT array and multi-walled CNTs, are underway.

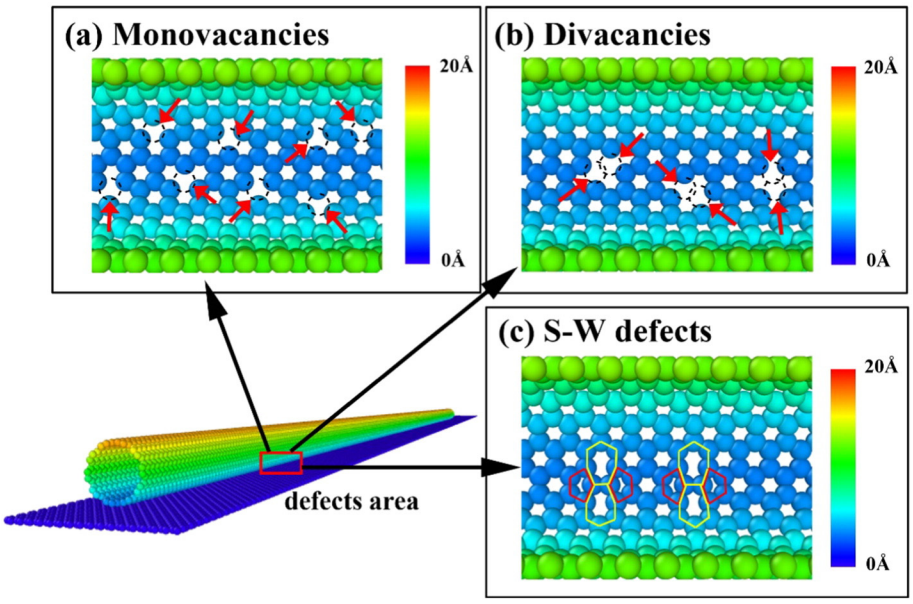

Fig. 10. Diagrammatic cross-section of CNTs containing different types of defects. The black dashed circles indicated by red arrows represent (a) monovacancies and (b) divacancies. (c) S-W defects of two pentagons are highlighted in red and those of two heptagons are highlighted in yellow. Carbon atoms are colored according to their z-coordinates. (For interpretation of the references to color in this figure legend, the reader is referred to the web version of this article.)

Prime novelty statement

This work further investigates the adhesion force of perfect CNTs and CNTs containing original and irradiation induced defects by molecular dynamics simulation. It also explains the microscopic mechanism of adhesive behavior between CNTs and graphene substrate, which is important for us to understand.

Acknowledgements

This work was supported by the Funding of Jiangsu Innovation Program for Graduate Education (Grant No. KYLX15_0306), the Fundamental Research Funds for the Central Universities (Grant No. NJ20150021), the Foundation of Graduate Innovation Center in NUAA (Grant No. kfjj201443), and the Priority Academic Program Development of Jiangsu Higher Education Institutions.

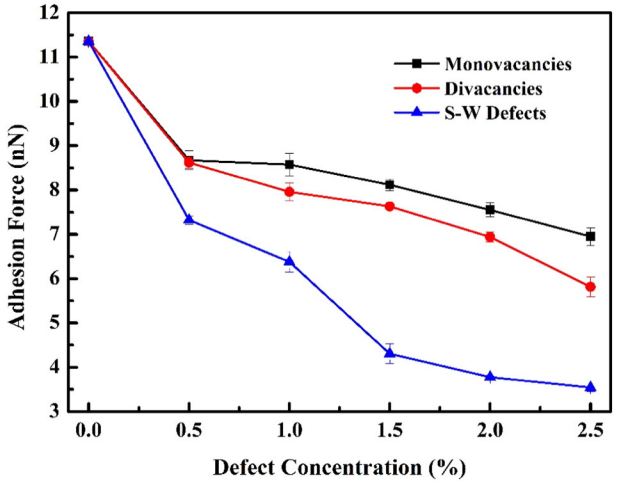

Fig. 11. Adhesion force of CNTs containing different types of defects as a function of the defect concentration.

References

[1] A. Jagota, C.Y. Hui, Adhesion, friction, and compliance of bio-mimetic and bio-inspired structured interfaces, Mater. Sci. Eng. R 72 (12) (2011) 253–292, http://dx.doi.org/10.1016/j.mser.2011.08.001.
[2] H.S. Im, K.Y. Kwon, J.U. Kim, K.S. Kim, H. Yi, P.J. Yoo, C. Pang, H.E. Jeong, T. Kim, Highly durable and unidirectionally stooped polymeric nanohairs for gecko-like dry adhesive, Nanotechnology 26 (41) (2015) 415301, http://dx.doi.org/10.1088/0957-4484/26/41/415301.
[3] S. Ma, D. Wang, Y. Liang, B. Sun, S.N. Gorb, F. Zhou, Adhesion: gecko-inspired but chemically switched friction and adhesion on nanofibrillar surfaces (small 9–10/2015), Small 11 (9–10) (2015) 1130, http://dx.doi.org/10.1002/smll.201570055.
[4] C.F. Schaber, T. Heinlein, G. Keeley, J.J. Schneider, S.N. Gorb, Tribological properties of vertically aligned carbon nanotube arrays, Carbon 94 (2015) 396–404, http://dx.doi.org/10.1016/j.carbon.2015.07.007.
[5] S.C. Roh, E.Y. Choi, Y.S. Choi, C.K. Kim, Characterization of the surface energies of functionalized multi-walled carbon nanotubes and their interfacial adhesion energies with various polymers, Polymer 55 (6) (2014) 1527–1536, http://dx.doi.org/10.1016/j.polymer.2014.02.015.
[6] M.R. Roenbeck, X. Wei, A.M. Beese, M. Naraghi, A. Furmanchuk, J.T. Paci, G.C. Schatz, H.D. Espinosa, In situ scanning electron microscope peeling to quantify surface energy between multiwalled carbon nanotubes and graphene, ACS Nano 8 (1) (2014) 124–138, http://dx.doi.org/10.1021/nn402485n.
[7] M.R. Roenbeck, A. Furmanchuk, Z. An, J.T. Paci, X. Wei, S.T. Nguyen, G.C. Schatz, H.D. Espinosa, Molecular-level engineering of adhesion in carbon nanomaterial interfaces, Nano Lett. 15 (7) (2015) 4504–4516, http://dx.doi.org/10.1021/acs.nanolett.5b01011.
[8] L. Ge, S. Sethi, L. Ci, P.M. Ajayan, A. Dhinojwala, Carbon nanotube-based synthetic gecko tapes, Proc. Natl. Acad. Sci. U. S. A. 104 (2007) 10792–10795, http://dx.doi.org/10.1073/pnas.0703505104.
[9] D. Leckband, J. Israelachvili, Intermolecular forces in biology, Q. Rev. Biophys. 34 (02) (2001) 105–267, http://dx.doi.org/10.1017/S0033583501003687.
[10] J. Buchoux, L. Bellon, S. Marsaudon, J.P. Aime, Carbon nanotubes adhesion and nanomechanical behavior from peeling force spectroscopy, Eur. Phys. J. B 84 (1) (2011) 69–77, http://dx.doi.org/10.1140/epjb/e2011-20204-1.
[11] T. Li, A. Ayari, L. Bellon, Adhesion energy of single wall carbon nanotube loops on various substrates, J. Appl. Phys. 117 (16) (2015) 164309, http://dx.doi.org/10.1063/1.4919355.
[12] Y. Zhao, T. Tong, L. Delzeit, A. Kashani, M. Meyyappan, A. Majumdar, Interfacial energy and strength of multiwalled-carbon-nanotube-based dry adhesive, J. Vac. Sci. Technol. B 24 (1) (2006) 331–335, http://dx.doi.org/10.1116/1.2163891.
[13] L. Qu, L. Dai, M. Stone, Z. Xia, Z.L. Wang, Carbon nanotube arrays with strong shear binding-on and easy normal lifting-off, Science 322 (5899) (2008) 238–242, http://dx.doi.org/10.1126/science.1159503.
[14] A. Buldum, Adhesion and friction characteristics of carbon nanotube arrays, Nanotechnology 25 (34) (2014) 345704, http://dx.doi.org/10.1088/0957-4484/25/34/345704.
[15] F. Chen, X. Tang, H. Huang, J. Liu, H. Li, Y. Qiu, D. Chen, Surface damage and mechanical properties degradation of Cr/W multilayer films irradiated by Xe 20^{+}, Appl. Surf. Sci. 357 (2015) 1225–1230, http://dx.doi.org/10.1016/j.apsusc.2015.09.170.

[16] H. Huang, X. Tang, F. Chen, Y. Yang, J. Liu, H. Li, D. Chen, Radiation damage resistance and interface stability of copper–graphene nanolayered composite, J. Nucl. Mater. 460 (2015) 16–22, http://dx.doi.org/10.1016/j.jnucmat.2015.02.003.
[17] S. Suzuki, Y. Kobayashi, Threshold energy of low-energy irradiation damage in single-walled carbon nanotubes, Jpn. J. Appl. Phys. 47 (4R) (2008) 2040, http://dx.doi.org/10.1143/JJAP.47.2040.
[18] S. Suzuki, Y. Kobayashi, Diameter dependence of low-energy electron and photon irradiation damage in single-walled carbon nanotubes, Chem. Phys. Lett. 430 (4) (2006) 370–374, http://dx.doi.org/10.1016/j.cplett.2006.08.143.
[19] M. Yasuda, Y. Kimoto, K. Tada, H. Mori, S. Akita, Y. Nakayama, Y. Hirai, Molecular dynamics study of electron-irradiation effects in single-walled carbon nanotubes, Phys. Rev. B 75 (20) (2007) 205406, http://dx.doi.org/10.1103/PhysRevB.75.205406.
[20] S.K. Pregler, S.B. Sinnott, Molecular dynamics simulations of electron and ion beam irradiation of multiwalled carbon nanotubes: the effects on failure by inner tube sliding, Phys. Rev. B 73 (22) (2006) 224106, http://dx.doi.org/10.1103/PhysRevB.73.224106.
[21] S. Plimpton, Fast parallel algorithms for short-range molecular dynamics, J. Comput. Phys. 117 (1) (1995) 1–19, http://dx.doi.org/10.1006/jcph.1995.1039.
[22] S.J. Stuart, A.B. Tutein, J.A. Harrison, A reactive potential for hydrocarbons with intermolecular interactions, J. Chem. Phys. 112 (14) (2000) 6472–6486, http://dx.doi.org/10.1063/1.481208.
[23] D.W. Brenner, Empirical potential for hydrocarbons for use in simulating the chemical vapor deposition of diamond films, Phys. Rev. B 42 (15) (1990) 9458, http://dx.doi.org/10.1103/PhysRevB.42.9458.
[24] D.W. Brenner, Erratum: empirical potential for hydrocarbons for use in simulating the chemical vapor deposition of diamond films, Phys. Rev. B 46 (3) (1992) 1948, http://dx.doi.org/10.1103/PhysRevB.46.1948.2.
[25] D.W. Brenner, J.A. Harrison, C.T. White, R.J. Colton, Molecular dynamics simulations of the nanometer-scale mechanical properties of compressed Buckminsterfullerene, Thin Solid Films 206 (1) (1991) 220–223, http://dx.doi.org/10.1016/0040-6090(91)90425-W.
[26] S. Ghosh, V. Padmanabhan, Adsorption of hydrogen on single-walled carbon nanotubes with defects, Diam. Relat. Mater. 59 (2015) 47–53, http://dx.doi.org/10.1016/j.diamond.2015.09.004.
[27] J. Guo, B. Wen, R. Melnik, S. Yao, T. Li, Molecular dynamics study on diamond nanowires mechanical properties: strain rate, temperature and size dependent effects, Diam. Relat. Mater. 20 (4) (2011) 551–555, http://dx.doi.org/10.1016/j.diamond.2011.02.016.
[28] A. Tolvanen, J. Kotakoski, A.V. Krasheninnikov, K. Nordlund, Relative abundance of single and double vacancies in irradiated single-walled carbon nanotubes, Appl. Phys. Lett. 91 (17) (2007) 173109, http://dx.doi.org/10.1063/1.2800807.
[29] Z. Xu, W. Zhang, Z. Zhu, P. Huai, Molecular dynamics study of damage production in single-walled carbon nanotubes irradiated by various ion species, Nanotechnology 20 (12) (2009) 125706, http://dx.doi.org/10.1088/0957-4484/20/12/125706.
[30] F. Banhart, J. Kotakoski, A.V. Krasheninnikov, Structural defects in graphene, ACS Nano 5 (1) (2010) 26–41, http://dx.doi.org/10.1021/nn102598m.